Experimental Investigations of Annular Liquid Curtains

K. D. Kihm
Department of Mechanical Engineering,
Texas A&M University,
College Station, TX 77843

N. A. Chigier
Mechanical Engineering Department,
Carnegie-Mellon University,
Pittsburgh, PA 15213

Experiments have been performed to study the dynamics of vertical annular liquid curtains. Using a high and a low speed photographic recording technique, different modes of curtain formation have been visualized: (a) nonpressurized curtain, (b) pressurized steady curtain, (c) pressurized oscillating curtain, and (d) punctured curtain. The velocity of the liquid was measured by an argon-ion laser Doppler velocimeter, and results were compared with free falling motion. The convergence length of the curtain was measured as a function of the pressure differential for different Froude and Weber numbers, and for different nozzle gap widths. The experimental data agree well with existing theoretical predictions for steady curtains. For harmonically oscillating curtains, the average values of minimum and maximum convergence lengths show fairly good agreement with the theory.

Introduction

When liquid emerges vertically downward from an annular nozzle, a conical liquid sheet, which will be called a "liquid curtain," is formed due to the combined effects of the contractive action of surface tension, the elongative action of inertia and gravity, and the expanding action of pressure differential between the inside and the outside of the curtain (Fig. 1). The convergence length L is defined as a distance from the nozzle exit to the apex of the liquid curtain.

The concept of utilizing a liquid curtain as a sealed reactor chamber was proposed for the design of an inertial confinement fusion (ICF) reactor to alleviate several problems associated with a solid reactor chamber (Maniscalco and Meier, 1977). Interest in the dynamics of liquid curtains has grown in connection with a proposed design of a system for direct reduction of zirconium from zirconium tetrachloride ($ZrCl_4$) and sodium (Na) (Chigier et al., 1987). The conventional Kroll process involves mixing of $ZrCl_4$ and Na by injecting them separately into a solid reactor chamber. The reduction efficiency of Zr is very low since the molecular diffusion force that drives Zr into a molten pool is weak. However, if the $ZrCl_4$ spray were surrounded by a curtain of liquid sodium so that the reduced Zr could be driven through the apex of the conical curtain, a viable reactor with an improved reduction efficiency would be achieved. The liquid curtain also prevents the escape and/or the evaporation of homogeneously formed zirconium.

The history of the quantitative study of liquid curtains goes back at least to the 19th century when Boussinesq (1869) proposed a mathematical model for water bells. Amongst many studies (Lance and Perry, 1953, and Taylor, 1959) that have been devoted to establish the relevant phenomena, Binnie and Squire (1941) first employed the basic models to derive nonlinear differential equations that describe the behavior of liquid curtains. The differential equations were simplified and analytically solved for the flow at zero pressure differential. The study of Baird and Davidson (1962) is based on a similar analysis, but accounts for the presence of pressure differential across the curtain. However, both of these studies did not account for the gravity effect, and assumed that the thickness of the liquid sheet is negligibly thin.

The analysis of Holvingh (1977) accounts for the effect of gravitational acceleration and derives a solution for the convergence length analytically. Hoffman et al. (1980) generalized and improved Holvingh's analysis by including the surface

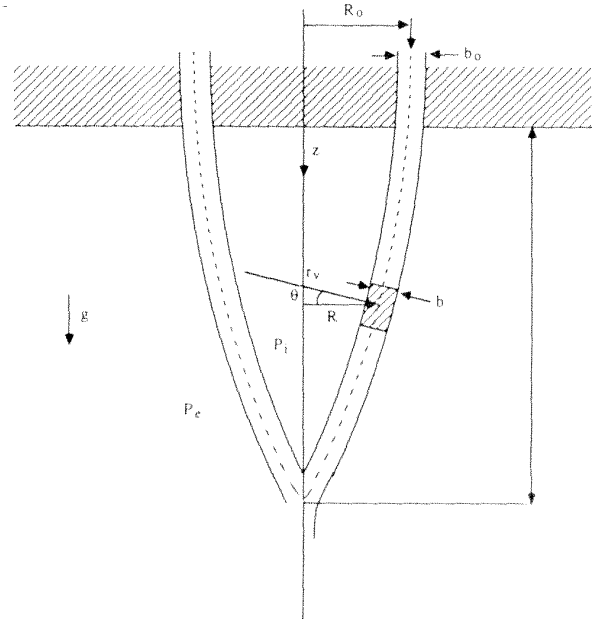

Fig. 1 Schematic diagram of liquid curtain from an annular nozzle

Contributed by the Fluids Engineering Division for publication in the Journal of Fluids Engineering. Manuscript received by the Fluids Engineering Division August 23. 1988.

tension forces from both the inner and the outer surfaces of the curtain. Experimental verification of the theory was also attempted and results showed good agreement with the calculated convergence length at low flow velocities. At high flow velocities, the measured lengths were found to be significantly shorter than the calculated lengths. It is believed that this is due to the enhanced contractive action driven by the flowinduced partial vacuum inside the curtain. Unfortunately, both of these studies did not consider the influence of the pressure differential on the convergence length.

A more rigorous theory was developed by Esser and Abdel-Khalik (1984) who were motivated by the recognition that no purely analytical model can simultaneously account for all of the flow parameters of interest. The two-dimensional, steadystate, parabolic Navier-Stokes equations were applied to the flowing liquid and solved for the velocity and pressure distributions using the finite-difference computer code ANNJET. The calculated results agreed well with the measured convergence length with zero pressure differential obtained by Hoffman et al. (1980). For curtains with a nonzero pressure differential, more extensive measurement is needed to confirm the validity of the theory.

Ramos (1988) modified the Lagrangian formulation originally developed by Hoffman et al. (1980), and obtained analytical and numerical solutions. The analytical predictions, in which the radius of curvature in the vertical plane is neglected assuming along curtain, showed longer convergence lengths than numerical predictions.

In the present study the convergence length is measured as a function of pressure differential $p_i - p_e$, for several combinations of the principal parameters: the ratio of the nozzle gap to the orifice radius b_o/R_o and initial liquid velocity V_o. The significant dimensionless parameters are the Froude number $Fr = V_o^2/gR_o$, the Weber number $W_e = \rho V_o^2 b_o /2\sigma$ where ρ and σ denote the liquid density and surface tension coefficient, respectively, and the pressure coefficient $C_p = Fr^2 (p_i - p_e /\rho V_o^2)$. The data have been compared with the analytical and numerical predictions obtained by Ramos (1988).

Using an argon-ion laser Doppler velocimeter, velocities of the flowing liquid have been measured and the results are compared with the theory for a long curtain with an approximation of $| dR/dz << 1$ where R is the local curtain radius and z is the axial distance. Also, the evolution of the liquid curtains is photographically visualized as the pressure differential is progressively increased. It is demonstrated that the pressure differential force plays a major role in determining the characteristics of liquid curtains.

Experimental Apparatus

A schematic of the experimental apparatus is shown in Fig. 2. Liquid is injected vertically downward through a cylindrical annular nozzle into a tank. The nozzle is mounted in a threedimensional traversing system which is positioned by computer-controlled

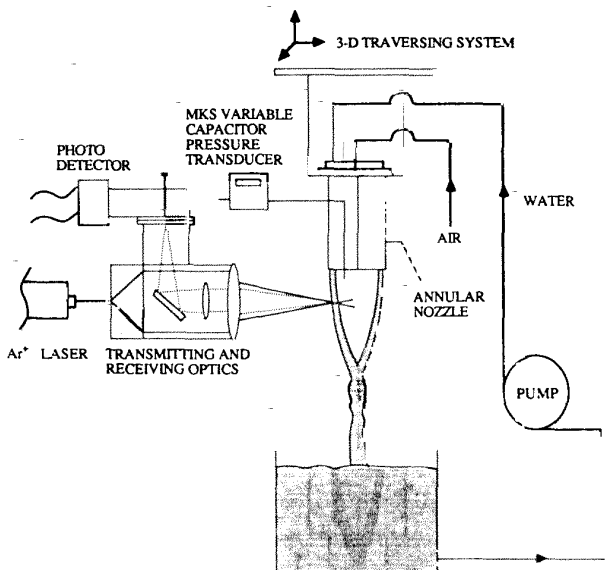

Fig. 2 Schematic diagram of experimental apparatus

stepping motors. Local tap water has been used for generating liquid curtains and the liquid is recirculated in a closed loop to maintain the same properties of the test fluid. The amount of natural seeding in the tap water was sufficient for providing good Doppler signals. Backward scattered signals from the LDA optical system were detected to avoid the attenuation of Doppler signals by the liquid curtain. The attenuation increases as the liquid velocity fluctuations in the curtain increase. The detected Doppler signal is processed by a counter type TSI 1980 processor and analyzed by a Digital MINC-23 data acquisition system. The anemometer was calibrated using a TSI calibrating wheel. The bias of the velocity measurement was found to be negligible and the discrepancy between the normal speed of the wheel and the actual measurement was less than 1 percent.

The nozzle designed for the study is shown in Fig. 3. Water is pumped through the annular nozzle after passing through a filter and a settling chamber. The variation of the annular nozzle gap is achieved by installing inserts of different sizes. The nozzle outer diameter is 100 mm and two different inserts are used to provide gap thicknesses of 0.5 mm and 1.0 mm. The length/gap width ratio is 80 (for the 0.5 mm gap width) so that the flow at the nozzle exit is developed to a fully annular flow. An air inlet is located at the center of the center piece and the air supply is maintained at various pressures in order to study the effect of pressure differential on the curtain shape and stability. The minute pressure difference between the inner and outer regions of the curtain is measured using a MKS 398H

Nomenclature

b = local curtain film thickness
b_o = initial curtain thickness or nozzle gap thickness
C_P = pressure coefficient $[Fr^2 (p_i - p_e)/ \rho V_o^2]$
Fr = Froude number $[V_o^2 / gR_o]$
g = gravitational acceleration
L = curtain convergence length
L^* = dimensionless convergence length $[L/R_o]$
N_c = convergence number $[\rho g^2 R_o b_o 2V_o^2 \sigma]$
Pa = Pascal
P_i = pressure inside the curtain
P_e = pressure outside the curtain
ΔP = pressure differential $[Pi - Pe]$
R = local curtain radius in the horizontal plane
R_o = initial curtain radius or nozzle outer diameter
r_v = radius of curvature of the curtain in the vertical plane
t = time
V = axial mean velocity (local)
V = axial mean velocity at the nozzle exit
V^* = dimensionless axial mean velocity $[V/V_o]$
We = Weber number $[\rho V_0 b_o / 2\sigma]$ z
z = axial distance
Z^* = dimensional axial distance $[z/R._o]$
ρ = liquid density
σ = surface tension coefficient
θ = angle between r_v and R in the vertical plane

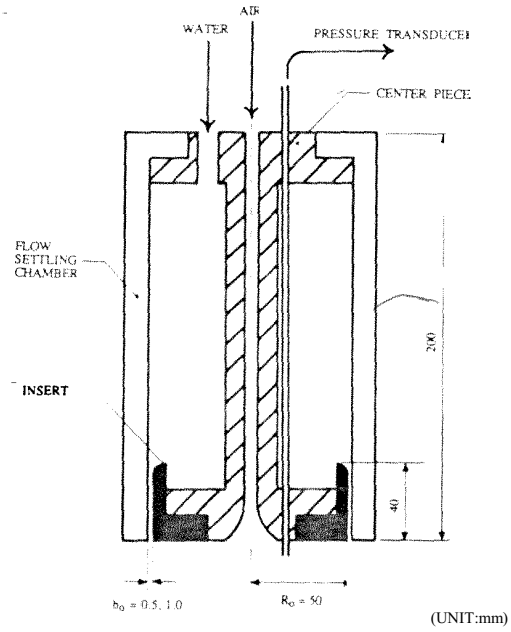

Fig. 3 Annular nozzle for generating liquid curtain

variable capacitor type differential pressure transducer with maximum range of I torr. By directly connecting the high and the low (ambient) pressure ports of the transducer, the zero calibration was checked within the accuracy of 10^{-3} Pascal. For oscillating curtains, the pressure readings fluctuated with time and the mean value was measured for an average pressure differential. According to the factory calibration performed with a pressure chamber and a dead weight, less than one percent of measurement is estimated for the bias of the instrument. The precision of the pressure differential measurement is estimated as three percent or less including the reading error from the digital display of the instrument.

Visualization of Liquid Curtains

The geometry of liquid curtains is shaped as a result of the combined effects of surface tension, gravity, inertia, and pressure differential. When these effects are in equilibrium, a curtain remains stable (steady or harmonically oscillating) until the balance is broken by a disturbance. As long as the magnitude of the disturbance is below a critical value, the curtain readjusts to a new equilibrium resulting in shorter or longer curtains. However, when the disturbance exceeds the critical value, the curtain is no longer able to maintain its closed and stable shape. Instead, the curtain collapses or is punctured near the apex. The primary length scale for curtain shape is the convergence L for a given nozzle geometry b_0/R_0.

The convergence length usually increases as the pressure differential is progressively increased. Typical modes of different curtain formations depending on the pressure differential are shown in Figs. 4(a) to 4(d). Without pressurization (Fig. 4(a)), slow reduction of the air inside the curtain driven by the flowing liquid through the apex results in a partial vacuum within the curtain with a small pressure differential. This pressure differential force plus surface tension act radially inward, which increases as the pressure continuously decreases nside the curtain. The convergence length decreases gradually and the curtain eventually collapses, unless the air supply is continued in order to compensate for the small amount of air entrained by the flowing liquid and, at the same time, to prevent the reduction in pressure inside the curtain.

In order to maintain a steady curtain, a small amount of air, which

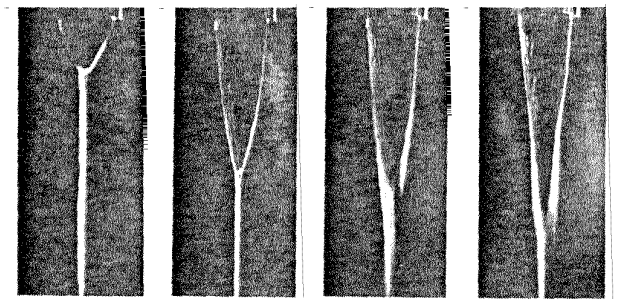

Fig. 4 Various types of liquid curtains

balances the air leakage, needs to be introduced into the curtain. The steady curtain (Fig. *4(b)) is* maintained as a result of the balance between the surface tension, pressure differential, inertial and gravitational forces. Inertial forces are axially downwards at the nozzle exit and for the period during which the curtain remains cylindrical. When the curtain begins to converge, which is caused by the contractive action of surface tension, a radially inward component appears in the inertial forces. By pressurizing the curtain, the pressure forces act radially outward causing an increase in the local diameter and thus extending the length of the cylindrical region until a new equilibrium between the forces is reached. Therefore, the more the curtain is pressurized, the longer the curtain (convergence) length.

When the curtain is pressurized with a pressure differential beyond a certain value, the contractive surface tensions can no longer hold the curtain steady because of the strong expanding action of the pressure forces. The curtain is expanded until the expansion reaches a limit in which the surface tensions start pulling the curtain upward (or radially inward). The curtain contracts until the contraction reaches the other limit in which the internal pressure becomes high enough to initiate an expansion of the curtain. As a result of this overshooting, the expansion and the contraction repeat like a simple harmonic oscillation attributed to the pressure fluctuation. A photograph of an oscillating curtain is shown in Fig. *4(c).* The exposure time for the camera aperture was two seconds. The recorded inside apex of the curtain represents one instant of time (minimum length) while the blurred section of the photograph is due to the curtain fluctuations which are of the order of 2 Hz.

When the pressure differential exceeds a critical value, the surface tension is not able to initiate the curtain convergence since the expanding pressure forces are high enough to override the contractive action of surface tension. This results in a sudden decrease in curtain length and internal pressure as shown in Fig. 4(d). The curtain must now be considered as an open ended flow system with a jet flow from the air nozzle on the axis to the punctured opening. Increasing the supply air pressure increases the flow rate of air through the system without raising the pressure inside the curtain. The curtain near the apex fluctuates with a high frequency of the order of 10 Hz. Kendall (1986) showed experimentally and Lee and Wang (1986) showed theoretically that at specific conditions a sealing-off and encapsulation of the core-gas results in spherical liquid shell formation.

Review of the Theory

Lance and Perry (1953) presented the general differential equations for a "water bell" based on the Lagrangian formulation using a tangential-normal coordinate system. Transforming the differential equations into a cylindrical coordinate system, Hoffman et al. (1980) derived the vertical and radial momentum equations valid for a thin jet with zero pressure differential. Ramos (1988) accounted for the effect of nonzero pressure differential and obtained similar differential equations for R (t) and z(t), i.e.,

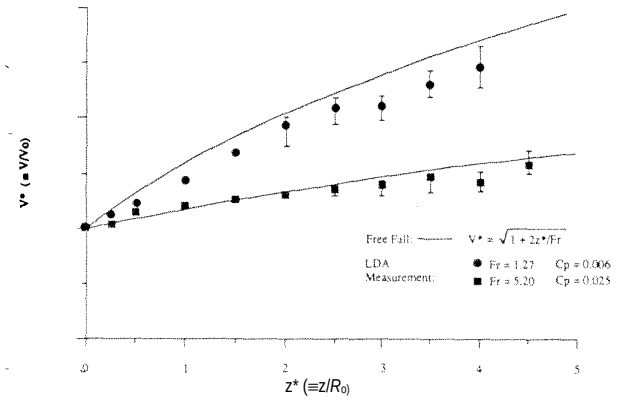

Fig. 5 Axial mean velocity normalized by the nozzle exit velocity V*(≡*V*/*V*$_o$) as a function of z* (≡*z*/*R*$_o$) for two different Froude numbers: *b*$_o$/*R*$_o$ = *0.01* and *Δp* = 2.4 Pa for *V*$_o$ = 0.8 m/s and 1.61 m/s

$$\frac{d^2R}{dt^2} = -\frac{2\sigma\cos\theta}{\rho b}\left(\frac{\cos\theta}{\rho b}+\frac{1}{r_v}\right)+\cos\theta(P_i-P_e) \tag{1}$$

$$\frac{d^2z}{dt^2} = g-\frac{2\sigma\cos\theta}{\rho b}\left(\frac{\cos\theta}{R}+\frac{1}{r_v}\right)+\sin\theta(P_i-P_e) \tag{2}$$

where r_v is the radius of curvature in the vertical plane at a particular axial location (Fig. 1), R is the local radius of the curtain in the horizontal plane and b is the local thickness of the curtain. The angle θ is defined in the vertical plane between the radius of curvature r_v and the curtain radius R.

The set of equations (1) and (2) together with the continuity and the curvature equation ($r_v = r_v(R, z)$) was solved analytically and numerically by Ramos (1988). A closed form of analytical solutions was obtained for a very long curtain that converges very slowly, i.e, $|dR/dz| << 1$ and $\theta = 0$. In his numerical approach, the angle θ was expressed as a function of t, R and z, and the resulting equations were numerically integrated. Both of these solutions are compared with the measured convergence lengths in Figs. 7 through 11.

Results and Discussion

Mean velocity components of the flowing liquid have been measured using an argon-ion laser Doppler anemometer and results are shown for two different flow rates with the same pressure differential but with different C_p because of different liquid velocities (Fig. 5). The laser beams were focused onto the center of the curtain width at each axial station. Since it is expected that a nonuniform velocity profile due to shear stress along the nozzle walls relaxes rapidly at a short distance from the nozzle exit, the velocity distribution is assumed to be uniform across the liquid film. The dimension of the LDA probe volume was 5 mm in length and 0.25 mm in diameter so that the average velocity across the film thickness (~ 0.5 mm) can be obtained at each measurement location. For most regions of the curtain, except for the convergence point, zero tangential velocity was measured at each measurement location showing that no swirl was generated in the nozzle or liquid film. There may have arisen some swirl at the convergence point because of the small radial dimension where the flow is almost three dimensional. The rms fluctuations of the liquid flow gradually increase with distance downstream but never exceed 10 percent. The flow unsteadiness is initiated by the shear between the liquid and nozzle inner walls. The gradual increase of the unsteadiness outside the nozzle is attributed to the role of air friction on the liquid sheet as a weak but nonnegligible force. The repeatability of the measurement was excellent near the nozzle exit. As indicated by the extended error bars, the uncertainty of mean velocity increased as the convergence point was approached.

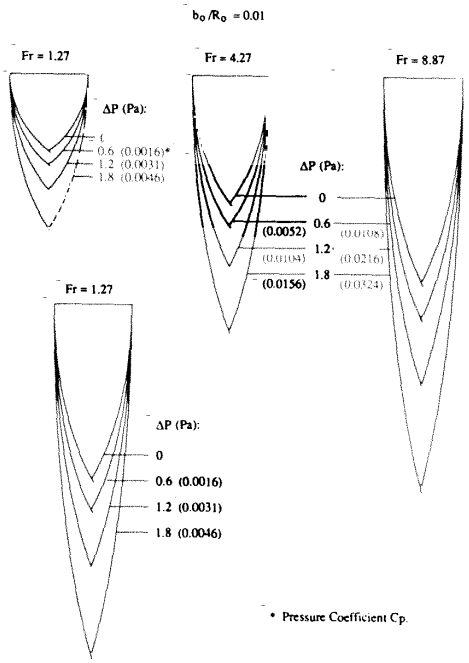

Fig. 6 Curtain shape and length as a function of ΔP(≡ Pi – P$_e$3) for three different Froude numbers and for two different values of *b*$_o$ /*R*$_o$.

Comparisons have been made between the measured velocities near the nozzle exit and the calculated mean velocities, based on the liquid mass flow rate. Good agreement was observed between the two values with the maximum deviations of 3 percent or less.

For a long curtain (θ=0), it can easily be seen from equation (2) that the axial velocity V(=dz/dt) is identical to the free falling velocity, i.e.,

$$V = V_o + gt \quad or \quad V^* = \sqrt{1+2z^*/Fr} \tag{3}$$

where the dimensionless velocity V^* and the axial coordinate z* are V/V_o and z/R_o, respectively. For the higher flow rate (Froude number = 5.20 and Weber number = 8.77), with an exit velocity of 1.6 m/s, the measured velocity agrees well with the free falling velocity, while the measured velocity for the lower flow rate (Fr = 1.27, We = 2.19 and Vo = 0.8 m/s) shows a lower value compared to the free falling velocity. The convergence length of the curtain increases as the flow rate is increased. The longer the curtain is, the more slowly the curtain radius R decreases with z ensuring the conditions $|dR/dz| << 1$ and $R << r_v|$, which validate the approximate solution for free falling velocity. This is clearly seen for the case of the longer curtain with Fr = 5.20. For the shorter curtain, these conditions are no longer valid since the curtain radius decreases faster, and the contractive action of surface tensions tends to retard the falling motion of the liquid resulting in a slower velocity than free falling.

The convergence length L^* ($\equiv L/R_o$) has been measured for the pressurized curtains which are either in the steady or oscillating mode using a photographic recording technique. For steady curtains, the exposure time of the camera aperture was 1/60 to 1/125 of a second. A longer time exposure of 0.5 to 2 seconds was applied for the oscillating curtain so that the average convergence length could be obtained from the minimum and the maximum curtain lengths of the multi exposed pictu re (Fig. 4(c)). The convergence length was measured using

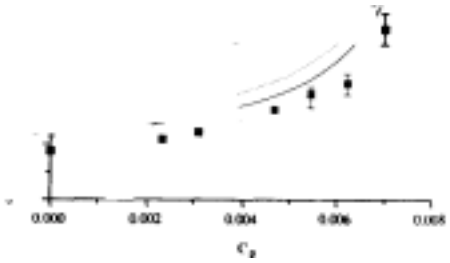

Fig. 7 Comparison of measured convergence length $L^*(\equiv L/R_o)$ versus C_p with theoretical predictions: $N_c = 1.34$ (Fr = 1.27 and We = 2.15), $b_o/R_o = 0.01$; ... analytical solution, —— numerical solution (Ramos [1988])

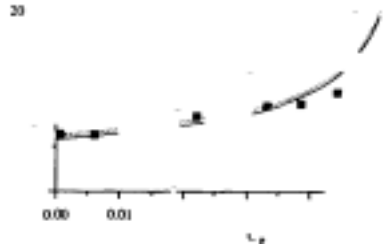

Fig. 9 Comparison of measured convergence length $L^*(\equiv L/R_o)$ versus C_p with theoretical predictions: $N_c = 0.19$ (Fr = 8.87 and We = 15.03), b_o/R_o = 0.01; ... analytical solution,—— numerical solution (Ramos [1988])

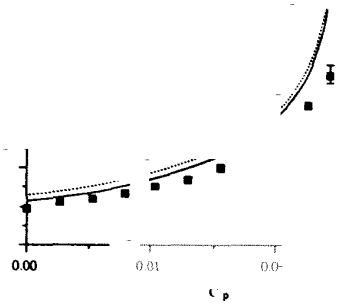

Fig. 8 Comparison of measured convergence length $L^*(\equiv L/R_o)$ versus C_p with theoretical predictions: $N_c = 0.40$ (Fr = 4.27 and We = 7.24), $b_o/R_o = 0.01$; ... analytical solution, —— numerical solution (Ramos [1988])

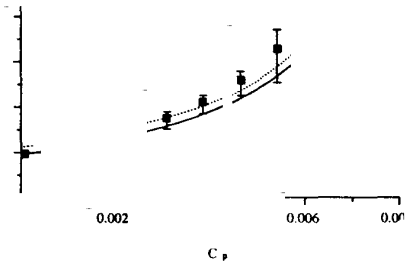

Fig. 10 Comparison of measured convergence length $L^*(\equiv L/R_o)$ versus C_p with theoretical predictions: $N_c = 2.67$ (Fr = 1.27 and We =4.31), $b_o/R_o = 0.02$; ... analytical solution,—— numerical solution (Ramos [1988])

a ruler with a minimum resolution of 1 mm, which was attached to the nozzle and photographically recorded together with each curtain. The precision of the measurement was estimated as I percent or less with the reading error of one half of the minimum resolution, i.e., 0.5 mm for most curtains that were longer than 5 cm.

The average length and shape of the inside surface of steady curtains recorded by photographs are plotted in scale in Fig. 6. In each case, the initial curtain radius is 50 mm. Figure 6 shows the progressive increase in length, local radius, and internal volume of the curtain as ΔP is increased. Figure 6 also shows the benefits in terms of greater stability, larger length, and larger internal volume which are attained when the gap width is doubled for the same Froude number. For each value of ΔP, the curtain length is steadily increased by increasing the liquid flow rate, velocity, and Froude number.

The measured convergence lengths compared with the predictions are shown for $b_o/R_{o=0.01}$ in Figs. 7 to 9 and for $b_o/R_{o=0.02}$ in Fig. 10. The symbol represents an averaged length of five individual recordings, while the extended bar indicates the range of measured lengths for each pressure differential. The nozzle radius R_o is fixed as a value of 50 mm for both cases. The solid curves represent the numerical solutions and the dashed curves denote the analytical solutions obtained from Ramos (1988). For all the cases considered, the numerical results predict a shorter convergence length compared to the analytical results. It is believed that the discrepancies between the two predictions are attributed to the terms including θ in the differential equations (1) and *(2).* In the numerical approach $\theta \neq 0$, while the analytical approach assumes $\theta = 0$ and neglects the contribution of surface tension in the second term on the right-hand side of equation *(2).* The major contribution of this term is to reduce both the falling velocity and the convergence length since the surface tension tends to hold the curtain, balancing the action of the gravitational and pressure differential forces. It can be seen from Figs. 7 to 9 that the discrepancies between the numerical and analytical solutions diminish as the flow rate is increased. For fixed nozzle geometry *(R_o* and *b_o)* and fluid properties (ρ and σ), both the Froude number and the Weber number increase with the flow rate. For long curtains with large flow rates, the angle θ becomes negligibly small in most regions except near the convergent apex. Therefore, the analytical solutions with $\theta = 0$ show close agreement with the numerical solutions as the Froude number and the Weber number increase with the flow rate. The influence of surface tension on the second term in equation (2) is very small for these cases.

The convergence length increases with increase of C_p, Fr, and We for a fixed value of $b_o/R = 0.01$. The variations of the convergence length with the pressure coefficient C_p show general agreement between the predictions and the measurements. For small values of C_p, curtains are steady with good repeatability of the measurements, and with good agreement with the theory. The curtain starts oscillating as the dimensionless pressure differential C_p increases. The lengths of the extended error bars are a measure of the magnitude of oscillation of the curtain apex, the convergence length. The degree of oscillation diminishes as the liquid flow rate is increased. This is due to the increased inertia overriding disturbances that cause the oscillation. For oscillating curtains, the unsteady formulation must be used to take into account the unsteady nature of the flow (Chigier et al., 1988).

The effect of b_o/R_o variation on the convergence lencth is shown in Fig. 10. Doubling the nozzle gap b_o, while kcrping the other parameters and dimensionless numbers the same, provides doubled mass and momentum flow rates. As expected, the convergence length is increased due to the increased

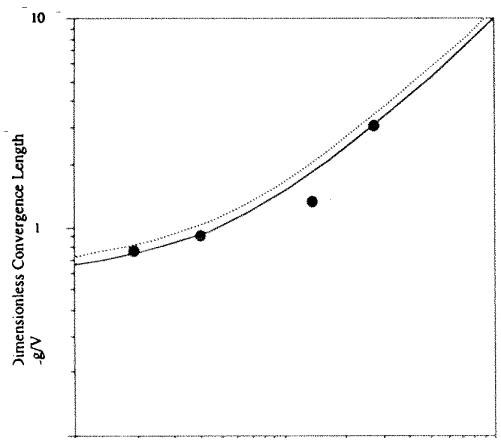

Flg. 11 Dimensionless convergence length Lg / Vo² versus convergence number Nc for Cp = 0: ● measured data; - - - analytical solution, and ——— numerical solution (Ramos (1988D

inertial (or momentum) forces. Compared to the similar condition but with the smaller nozzle gap of Fig. 6, the convergence length for low pressure differential has been nearly doubled. As we increase the pressure differential, the convergence length increases faster and has been almost tripled when C_p reaches 0.006. Again, the deviation of the predictions from the measurement increases as the curtain starts oscillating.

The dependence of convergence length upon the convergence number N_c which is defined as $N_c = \rho g^2 \ R_o^2 \ b_o / 2V_0^2 \ \sigma$ (≡ We / Fr^2), is examined in Fig. 11. For the case of zero pressure differential, i.e., $C_p = 0$, the dimensionless convergence length Lg / V_o^2 increases with the convergence number N_c showing close agreement between the measurement and the predictions. It must be emphasized that the convergence number is not the only parameter that determines the convergence length. The pressure coefficient C_p as well as N_p must be included in determining the convergence length of pressurized liquid curtains.

Conclusions

The dynamics of liquid curtains have been investigated by studying the convergence length and liquid velocity distributions experimentally. The experimental data have been compared with the analytical and numerical predictions of Ramos (1988). Also, different modes of curtain formation have been characterized using a photographic visualization technique. The main conclusions are listed below:

1. Steady curtains are formed when a steady pressure is maintained inside the curtain by providing a small air supply to compensate for the air leakage. As the pressure differential $P_i - P_e$ is increased, the curtain starts oscillating, and the curtain will be punctured above a critical pressure differential.

2. It has been shown that the convergence length of liquid curtains progressively increases with pressure coefficient C_p, Froude number Fr, Weber number We and nozzle gap to radius ratio b_0 / R_0. For the case of $C_p = 0$, the dimensionless convergence length Lg/V_o^2 increases with the increase of the convergence number N_c.

3. For steady curtains, both analytical and numerical models provide good predictions of convergence length showing fairly good agreement with the experimental results. The theory deviates from the measurement for oscillating curtains since the modeling is based on curtains with steady flow.

4. Laser Doppler velocimetry measurements show that the curtain flow is in free falling motion when the Froude number is high (Fr = 5.20). When the Froude number is low (Fr = 1.27), the liquid falling velocity was measured to be lower than that of free fall due to the enhanced holding action of surface tension.

Acknowledgments

The authors gratefully acknowledge the assistance of and discussions with Frank Sun, Zalman Shapiro, and Mike Roidt. Financial assistance was provided by DOE Basic Energy Sciences.

References

Abramowitz, M., and Stegun, I. A., 1972, *Handbook of Mathematical Functions,* Dover Publications Inc., 1962.

Baird, M. H. I., and Davidson, J. F., "Annular Jets-I (Fluid Dynamics)," *Chem. Eng. Sci.. Vol.* 17, 1941, pp. 467-472.

Binnie, A. H., and Squire, H. B., 1941, "Liquid Jets of Annular CrossSection," *The Engineer, Vol.* 171, London, 1941, pp. 236-238.

Boussinesq, J., 1869, "Comptes Rendus de I'Academie des Sciences," Vol. 69, p. 128.

Chigier, N. A., Ramos, J. I., and Sun, T-Y. 1987, "Experimental and Theoretical Studies of Vertical Annular Liquid Jets," Technical Report No. 1 prepared for the U.S. Department of Energy. Department of Mechanical Engineering, Carnegie-Mellon University, Pittsburgh, PA.

Chigier, N. A., Ramos, J. I., and Kihm, K. D., 1988, "Experimental and Theoretical Studies of Vertical Annular Liquid Jets," Technical Report No. 2 prepared for the U.S. Department of Energy. Department of Mechanical Engineering, Carnegie-Mellon University, Pittsburgh, PA.

Esser, P. D., and Abdel-Khalik, S. I., "Dynamics of Vertical Annular Liquid Jets," ASME Journal of Fluids Engineering, Vol. 106, 1980, pp. 45-51.

Hoffman, M. A., Takahashi, R. K., and Monson, R. D., 1980, "Annular Liquid Jet Experiments," ASME Journal of Fluids Engineering, Vol. 102, 1980, pp. 344-349.

Holvingh, J., 1977, "Stability of a Flowing Circular Annular Liquid Curtain with a Vertical Axis Subjected to Surface Tension Forces," Internal Memorandom No. 598A-77-108, Lawrence Livermore National Lab., Calif.

Kendall, J. M., 1986, "Experiments on Annular Liquid Jet Instability and on the Formation of Liquid Shells," Phys. *Fluids, Vol.* 29, pp. 2086-2094.

Lance, G. N., and Perry, R. L., "Water Bells," *Proceedings of the Physical Society,* London, Series B, Vol. 66, 1953, pp. 1067-1072.

Lee, C. P., and Wang, T. G., 1985, "A Theoretical Model for the Annular Jet Instability," Phys. *Fluids, Vol.* 29, 1977, pp. 2076-2085.

Maniscalco, J. A., and Meier, W. R., 1977, "Liquid Lithium 'Waterfall' Inertial Confinement Fusion Reactor Concept," Transactions of the American Nuclear Society, Vol. 26, 1977, pp. 62-63.

Ramos, 1. 1., 1988, "Liquid Curtains: 1. Fluid Mechanics," *Chemical Engineering Science* (in press).

Taylor, G. 1., 1959, "The Dynamics of Thin Sheets of Fluid. 1. Water Bells," *Proceedings of the Royal Society,* Series A, Vol. 253, 1959, pp. 289-295.